Langmuir

Article

pubs.acs.org/Langmuir

Self-Directed Growth of Aligned Adenine Molecular Chains on Si(111)7×7: Direct Imaging of Hydrogen-Bond Mediated Dimers and Clusters at Room Temperature by Scanning Tunneling Microscopy

Avisek Chatterjee, Lei Zhang, and K. T. Leung*

WATLab and Department of Chemistry, University of Waterloo, Waterloo, Ontario N2L 3G1, Canada

Supporting Information

ABSTRACT: The early stage of adsorption of adenine on Si(111)7×7 is studied by scanning tunneling microscopy (STM). Bright protrusions are observed in both empty-state and filled-state STM images, indicative of molecular adsorption of adenine through dative bonding. The majority of these bright protrusions appear as dimer pairs formed by hydrogen bonding at the initial adsorption stage. The formation of dative bonds between the substrate and adenine and the feasibility of the H-bond mediated dimers are supported by ab initio DFT/B3LYP/6-31G++(d,p) calculations, and are in excellent accord with our recent X-ray photoemission data. Remarkably, these dimers are found to undergo self-organization into aligned superstructures, evidently with common link arrangements, including straight, offset, and zigzag chains, square quartets, double quartets, and other multiple dimer structures. As the exposure of adenine increases, the populations of dimers as well as the self-organized double dimer and other higher-order structures also increase. The end-to-end dimer links are found to be most prominent in the growth of adenine molecular chains, most notably aligned along the Si dimer-wall or [−1 1 0] direction of the 7×7 unit cell. The self-aligned adenine dimer molecular chains offer a natural template for catch-and-release biosensing, lithography, and molecular electronic applications.

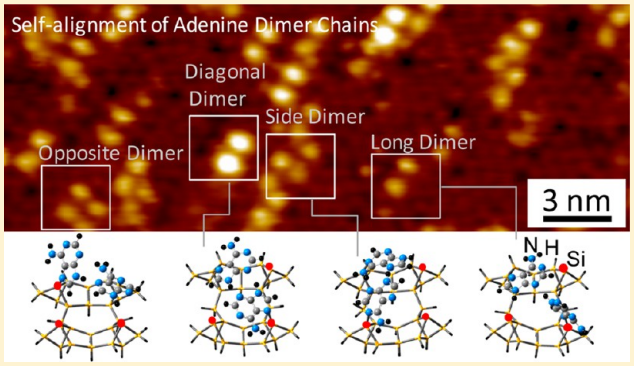

1. INTRODUCTION

In order to make new molecular scale devices, the need for incorporating organic functions into existing technologies has long been recognized. Understanding the growth of organic molecules on and their interactions with a common semiconductor surface (e.g., Si) represents the first step in developing molecular devices.[1,2] Organic functionalization could significantly extend the present silicon-based device technology especially as the device size is approaching the molecular scale. Single-molecule detection and multispecies chemical sensing, molecular photonics and electronics, and DNA-based biomolecular computing are just some of the emerging applications of bio/organic functionalization. To date, most of bio/organic functionalization of Si substrates involve bifunctional and multifunctional organic molecules, with nitrogen-containing functional groups (amines, amides) and oxygen-containing functional groups (carboxylic acids, alcohols) connected to an aliphatic backbone or to an aromatic ring structure (including benzene and their derivatives).[1] We have studied the surface chemistry of a series of bifunctional aliphatic molecules, including di- and per-chloroethylenes, dibromoethylene, acrylic acid, and propanoic acid,[3] allyl alcohol, allyl aldehyde, and allylamine[4] on Si(100)2×1, and difluoroethylene, dichloroethylenes, and more recently glycine on Si(111)7×7.[5] In the case of aromatic molecules, the aromatic ring could interact with the surface through cycloaddition reactions as in benzene and toluene, and through reactions with the heteroatom as in pyrrole, thiophene, and pyridine[6] on Si(100)2×1 and Si(111)7×7. The aromatic backbone can therefore act as an "anchor" to the surface, making the derivatives of these aromatic molecules with one or more appropriate functional groups excellent linker molecules (e.g., chlorobenzenes and dihalogenated benzenes).[7] While the interactions of multifunctional aliphatic molecules with the surface often involve covalent bonding, multifunctional heterocyclic aromatic molecules could also bind to the surface by dative bonding involving, e.g., the heteratom(s). The relatively moderate interaction as mediated by a dative bond not only preserves the molecular identity of the adsorbates but also facilitates their self-organization and initiation of film growth. This type of dative bonding therefore provides a different mechanism of anchoring the adsorbate to the surface, allowing all the functional groups on the ring backbone to interact with the surface with one another (as in, e.g., molecular folding), with other adsorbates (such as self-organization), and with other incoming species (acting as a linker molecule or undergoing biomolecular reactions).

Received: March 3, 2013
Revised: May 6, 2013
Published: May 6, 2013

   dx.doi.org/10.1021/la400775e | Langmuir 2013, 29, 9369−9377

Unlike metal surfaces, semiconductor surfaces offer directional bonds that are sufficiently strong to "trap" adsorbates at room temperature, eliminating the need to reduce the surface mobility of the adsorbates at low temperature (as on metal surfaces). The 7×7 reconstructed surface of Si(111) offers different types of dangling bond sites in the dimer-adatom-stacking fault model, with each unit cell consisting of 12 adatoms in the first layer, 6 restatoms in the second layer, and 1 corner-hole atom in the third layer.[8,9] The differences in the formal charges of a center adatom or CA (∼+1), a corner (Latin: *angulus*) adatom or AA (+7/12), and a restatom or RA (−1) contribute to their site-specific reactivities. On the other hand, the 2×1 reconstructed surface of Si(100) provides a lesser variety of dangling bond sites, with each unit cell consisting of 1 up and 1 down atoms each with two dangling bonds in the asymmetric dimer model.[3] In the present work, we focus on site-specific chemistry of the Si(111)7×7 surface that is generally considered less reactive than Si(100)2×1 but has a wider variety of bonding sites to accommodate different adsorbate structures.

To date, there have been a lot of recent STM studies on organic adsorbates on Si(111)7×7, including formic acid,[10] methanol,[11] trimethylphosphine,[12] pyrrole,[13] thiophene,[14] tetracene,[15] naphthalene,[16] and glycine.[17] Of the four DNA base molecules: adenine (Ade), guanine, thymine, and cytosine, Ade is the only nucleobase molecule without any oxo group, which reduces the basicity of the amino purines, making Ade more basic (pK_a = 4.2) than guanine (pK_a = 3.3). Ade is also the most aromatic nucleobase, with the aromaticity following the decreasing order: Ade > guanine > cytosine > thymine.[18] Unlike the other three nucleobases, Ade has only one functional group, i.e., the basic amino ($-NH_2$) group, making it the only available linking point with other species if the ring N atoms are involved in anchoring to the surface. Among the four nucleobases, Ade also has the largest number of ring N atoms capable of dative bonding.[3] Of the three types of N atoms in Ade, there are three pyridinic N1, N3, N7 (H-bond acceptors), one pyrrollic N9, and one amino N10 (H-bond donors), all of which could form H bond(s) with complementary H-bond donors or acceptors in other Ade or nucleobases such as thymine. The higher electron densities at the pyridinic N atoms make these N atoms more likely to form dative bonding with the surface.

Despite their importance, the surface chemistry and early adsorption of Ade and indeed other nucleobase molecules on Si(111)7×7 remain unknown. Only four studies on the adsorption of Ade and other nucleobases on other surfaces, Si(100)2×1, Cu(111), and Cu(110), have been reported. In particular, adsorption of Ade on Si(100)2×1[19] and of Ade and thymine together[20] have been studied by Kasaya et al. using STM and semiempirical molecular orbital calculations over 15 years ago. From their limited STM images at 0.02 ML (that do not reveal the Si dimer rows before Ade exposure), they concluded the existence of dimers on the surface with strong interaction with the surface. Even with their companion semiempirical calculations, these rather low-quality STM images did not allow the authors to provide a clearer picture about the adsorption. Later, Furukawa et al. studied the adsorption of all four nucleobases on the Cu(111) surface at ∼80 K by STM and reported that, except for the randomly oriented thymine, the other nucleobases form unique 2D structures on the surface.[21] Based on their molecular orbital calculations involving H bonding of two identical nucleobase molecules, they suggested that H-bonding could direct the growth of the 2D structures. Adsorption of Ade on Cu(110) has also been studied by Chen et al. at selected coverages above 0.08 monolayer by low energy electron diffraction, STM, and electron energy loss spectroscopy, along with ab initio calculations.[22] These authors concluded that Ade forms ordered $\begin{pmatrix} 1 & 2 \\ 6 & 0 \end{pmatrix}$ H-bonded structures after annealing an adenine-saturated surface at 430 K.

Recently, we studied the adsorption and growth evolution of benchmark molecules of fundamental biological interest, including glycine (the simplest amino acid)[5,17] and glycylglycine (the simplest peptide),[23] by STM and X-ray photoelectron spectroscopy (XPS). Both glycine and glycylglycine are found to exhibit strong interactions with the dangling-bond sites of the 7×7 surface, preventing them from self-organization upon adsorption. In the present work, we investigate the adsorption of Ade on Si(111)7×7 for the first time by using STM and ab initio calculations based on the density functional theory (DFT). Our STM results show that Ade undergoes self-organization of dimers, quartets, and higher-order superstructures along the Si dimer walls on the 7×7 surface. We also show that H-bonding plays a key role in the formation of these self-organized adsorbate structures. The site-specific information about the adsorption is in good accord with the local chemical-state information provided by our recent XPS study (Supporting Information).

2. EXPERIMENTAL AND COMPUTATIONAL DETAILS

All the experiments were performed in a five-chamber ultrahigh vacuum system (Omicron Nanotechnology, Inc.), equipped with a variable-temperature scanning probe microscope and an X-ray photoelectron spectrometer, along with a low-temperature organic effusion cell (Dr. Ebert MBE-Komponenten GmbH) for Ade deposition.[5] Single-side polished Si(111) chips (11× 2 mm^2, 0.3 mm thick) with a resistivity of 5 mΩ cm (Virginia Semiconductor, Inc.) were used as the substrates. A Si(111)7×7 reconstructed surface could be obtained by first outgassing at 400 °C overnight followed by flash-annealing at 1200 °C, and the resulting contaminant-free surface was easily verified by STM. Ade (Adrich, 99% purity, mp 360−365 °C) was deposited onto the Si substrate by thermal evaporation at an effusion cell temperature of 110 °C. The cracking patterns of Ade vapor were determined before and after deposition onto the Si substrate by a quadrupole mass spectrometer and they were found to be in good accord with that of Ade,[24] indicating that the Ade molecules remained intact in the gas phase upon evaporation at 110 °C. All the STM images were collected with an electrochemically etched, atomically sharp W tip at room temperature in a constant current mode at 150 pA tunneling current and a bias voltage of +2 V (empty-state imaging) and of −2 V (filled-state imaging).

All the calculations have been performed with the DFT method using the hybrid B3LYP functional in the *Gaussian 09* software package.[25] The hybrid B3LYP functional consists of Becke's 3-parameter gradient-corrected exchange functional[26] and Lee−Yang−Parr correlation functional.[27] The B3LYP functional has been found to provide generally good agreement with experimental results for the adsorption of organic molecules on a number of surfaces.[28,29] In the present work, we employed different split-valence basis sets for the equilibrium structure and frequency calculations. The 6-31G++(d,p) basis set was found to provide the lowest total energy and to be more appropriate for modeling hydrogen bonded (ad)species, with the counterpoise energy corrections for the basis set superposition error (BSSE). The dimerization energy calculations for adenine is performed by following the work of Hobza and Sponer.[30] Although their calculation involved dimerization of the DNA base molecules (adenine, guanine, cytosine, and thymine), our work provides all the possible configurations of adenine dimers. Planar molecules such as

dx.doi.org/10.1021/la400775e | *Langmuir* 2013, 29, 9369−9377

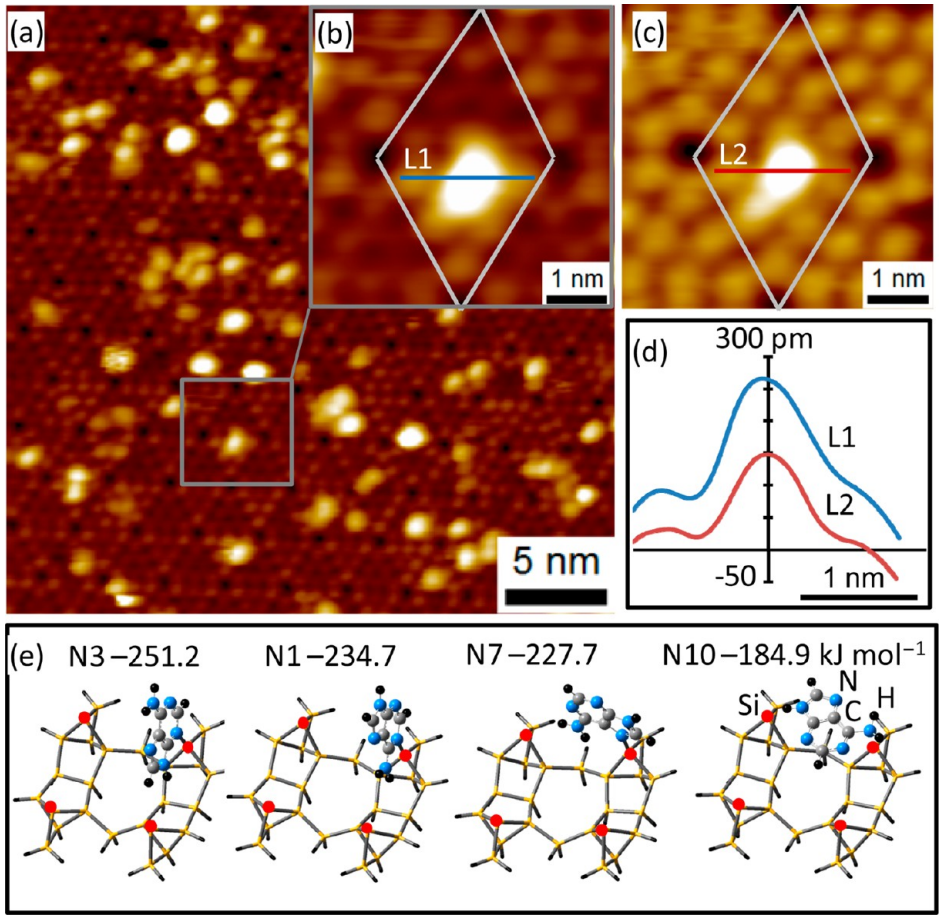

Figure 1. (a) Filled-state STM image (30 × 30 nm^2) of adenine adsorbed on Si(111)7×7 obtained with a sample bias of −2 V and a tunneling current of 150 pA; (b) the filled-state image; and (c) empty-state image (both 5 × 5 nm^2) of a selected 7×7 unit cell with a single adenine molecule adsorbed as marked by the square box in (a); (d) the height profiles along linescans L1 and L2 in (b) and (c), respectively; and (e) equilibrium adsorption geometries and their corresponding adsorption energies (in kJ mol^{-1}) of a single adenine molecule datively bonded through the N1, N3, N7, or N10 atom to a $Si_{26}H_{24}$ cluster (with the Si adatoms marked by solid circles), as optimized by the DFT/B3LYP/6-31++G(d,p) method.

benzene and arenes, including the nucleobases, were found to have nonplanar ground-state geometries as predicted by the typical ab initio methods (e.g., DFT, MP2, MP4) when combined with the standard Pople's basis sets. These inconsistencies could be explained in terms of intramolecular basis set superposition errors as reported in the literature. For Ade, a similar approach has been adopted to deal with the problems of spurious imaginary frequencies found for the optimized ground-state geometries with these methods (DFT, MP2) by the counterpoise energy corrections. The counterpoise energy corrections could be calculated by considering the different components inside the Ade molecule, including the diatomic N—H and C═C components and the larger N═C—NH_2 and N═CH components with the unsaturated N atoms. We considered the latter larger components to be in high spin states as reported in the literature.[31] In accord with the dimer-adatom-stacking-fault model proposed for the Si(111)7×7 surface by Takayanagi et al.,[32] a $Si_{26}H_{24}$ cluster was used to represent the double adatom−adatom pair across the dimer wall, with the adatom−adatom separation constrained at 6.65 Å. This considerably larger cluster was built upon the $Si_{12}H_{12}$ cluster commonly used in the literature to model a single adatom−adatom pair.[33] Developed by us for this type of problems, this larger cluster was found to be essential for simulating H-bonding interactions between two (Ade) adspecies. Except for the four top Si adatoms, all the Si atoms in the $Si_{26}H_{24}$ cluster were terminated with H atoms, and the cluster was optimized at the DFT/B3LYP/6-31G++(d,p) level. A full frequency calculation was also performed after each geometry optimization at the same level of computation, and no imaginary frequencies were found for the optimized adstructures.

3. RESULTS AND DISCUSSION

Figure 1a shows a typical filled-state STM image for a 10 s exposure of Ade on Si(111)7×7. Each bright protrusion of the 30 × 30 nm^2 image represents an individual Ade molecule adsorbed on the surface. Evidently, approximately half of the bright protrusions appear individually on adatom sites (with a preference for center adatoms) while the other half appear in groups. A magnified filled-state image of an Ade molecule (single) adsorbed at a center adatom site on the faulted half of the 7×7 unit cell (Figure 1b) is found to be quite similar to the corresponding empty-state image (Figure 1c). In particular, the adsorbed Ade appears as a bright protrusion in both images. The corresponding height profiles along linescans L1 and L2 (Figure 1d) show that the height above a neighboring Si adatom for filled-state (270 pm) is larger than that for empty state (150 pm), which is attributed to a higher local density of states (LDOS) associated with the filled states of the adsorbed Ade. Evidently, both the filled-state and empty-state images show that the adsorption of Ade does not produce any correlated bright−dark features as found in the STM images for glycine adsorption,[17] which indicates the differences in the nature of their adsorption. In particular, glycine undergoes N−H dissociative adsorption through the formation of N−Si bond that leads to a bright protrusion in the STM image, while the formation of Si−H bond resulting from the dissociated H atom

dx.doi.org/10.1021/la400775e | Langmuir 2013, 29, 9369−9377

generates a corresponding dark depression in the nearest-neighboring restatom site. The lack of correlated bright−dark features in the STM images for Ade adsorption therefore suggests that H dissociation does not occur in the adsorption process. This is in good accord with our recent XPS study that shows the formation of N→Si dative bonds for Ade adsorption on the 7×7 surface, as supported by the presence of the corresponding N 1s feature at 401.1 eV (Supporting Information).

Figure 1e shows four possible calculated adsorbate−substrate configurations (ASCs) of Ade adsorbed on the $Si_{26}H_{24}$ model surface through the formation of dative bonding between different N atoms and a Si adatom, all optimized at the DFT/B3LYP/6-31++G(d,p) level. We identify the different adstructures as Nn by the n-position of the N atom in Ade that forms the dative bond, along with their adsorption energies in Figure 1e. We could rule out dative bonding from the pyrrolic N (N9) because its lone-pair electrons are involved in the ring aromaticity.[34] The ASC N3 with an adsorption energy of −251.2 kJ mol^{-1} is found to be comparable in stability to ASC N1 (−234.7 kJ mol^{-1}) and N7 (−227.7 kJ mol^{-1}). The ASC N10 (−184.9 kJ mol^{-1}) is less stable than the other three due to delocalization of electrons from the $-NH_2$ group to the ring, which reduces the basicity of the amino group. On the other hand, the higher electron densities associated with the 1, 3, and 7 positions of the Ade ring give rise to the formation of more stable datively bonded products. In order to maximize the bonding between the N ring atoms and the Si adatom, ASC N3, N1, and N7 are found to have less tilted geometries (with the ring axis near perpendicular to the surface plane), in contrast to ASC N10 (involving the $-H_2N$→Si dative bonding) with the ring axis nearly parallel to the surface plane. Figure 1a also shows that the single protrusions could appear with different sizes and different degrees of brightness, which could be attributed to different extents of the molecular tilt with respect to the surface normal. This is consistent with the adsorption dynamics study of acetylene on Pd(111) reported by Dunphy et al.,[35] who observed that the relative size of the protrusion increases with the molecular tilt due to better overlap of the π orbital of acetylene with the STM tip. When the molecular axis of acetylene is perpendicular to the surface (zero tilt), the negative and positive lobes of its π orbitals cancel out the overlap with the (s) orbitals of the tip, resulting in dark depression in the STM image. The molecular tilt in molecules with π orbitals (such as Ade) could therefore give rise to single protrusions with different brightness and sizes.

In addition to the singles, Figure 1 also reveals pairs of bright protrusions corresponding to dimers. To understand the formation of these dimers, we also performed DFT/B3LYP/6-31++G(d,p) calculations of "free" hydrogen-bonded Ade dimers. Similar DFT-based calculations were performed by Preuss and Bechstedt on adenine adsorbed on Cu(110) surface to account for the self-assembly of the adenine-dimer chains.[36] They have concluded that hydrogen bonding is the driving force for the formation and stability of the molecular overlayer. Figure 2 shows the possible hydrogen bonding arrangement among the pyridinic (N1, N3, N7), pyrrolic (N9), and amino groups (N10) in two isolated Ade molecules. Appropriate isodensity surface plots of the total electron densities of the dimers are also shown in order to illustrate their approximate shapes. The most stable H-bonded dimer A (Figure 2a) involves the N9−H···N3 and N3···H−N9 H-bonds, with the dimerization energy of −67.3 kJ mol^{-1}. In this notation, we represent the H-bond between two different components in two Ade monomers by a triple dot (···), and we define the dimerization energy Δ as the difference between the total energy of the H-bonded dimer, with counterpoise energy correction, and twice the total energy of a monomer. The next stable set of dimers involves N10−H···N3 and either N1···H−N9 (B1, with Δ = −53.8 kJ mol^{-1}, Figure 2b) or N7···H−N9 (B2, with Δ = −49.5 kJ mol^{-1}, Figure 2c). This is followed by the next group of dimers with H-bonds involving amino groups from both monomers: C1 with N10−H···N1 and N1···H−N10 (Δ = −42.3 kJ mol^{-1}, Figure 2d), C2 with N10−H···N1 and N7···H−N10 (Δ = −39.8 kJ mol^{-1}, Figure 2e), and C3 with N10−H···N7 and N7···H−N10 (Δ = −36.3 kJ mol^{-1}, Figure 2f). The stability of the dimers therefore appears to be inversely related to the number of H-bonds involving the amino group, with A (no amino group) > B1, B2 (one amino group) > C1, C2, C3 (two amino groups). The next least stable group of dimers involves one H-bond and one H-bond-like interaction between an N and a H−C groups, with D1 with N9−H···N7 and N3···H−C8 (Δ = −35.9 kJ mol^{-1}, Figure 2g) being more stable than D2 with N10−H···N1 and N7···H−C2 (Δ = −18.9 kJ mol^{-1}, Figure 2h). Finally, the least stable dimer E1 involves only H-bond-like interactions, with C8−H···N7 and N7···H−C8 (Δ = −13.0 kJ mol^{-1}, Figure 2i).

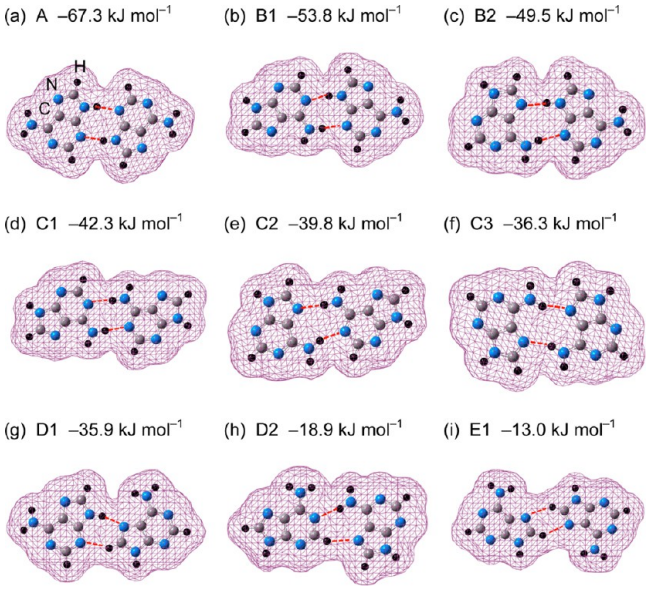

Figure 2. Equilibrium geometries and the dimerization energies of the hydrogen-bonded adenine dimers involving different N atoms (a−f) and C atoms (g−i), obtained by the DFT/B3LYP/6-31++G(d,p) method with counterpoise energy corrections to the basis set superposition errors.

It is of interest to note that of the more stable dimers involving only H-bonds (A, B1, B2, C1, C2, C3), it is more feasible to place two dimers end-to-end (with the long side of the dimer, i.e., along the H-bond direction, oriented back to back) rather than side-by-side (with the long side of the dimer oriented in parallel next to each other), because of the more ready availability of free N atoms at the ends of the dimers than on the sides. This type of interdimer interaction for such an end-to-end double dimer, usually with just a single interdimer H-bond, is expected to be weaker than the intradimer interaction within a single dimer with two H-bonds. While the dimer is a stable natural building block unit, a group of

dx.doi.org/10.1021/la400775e | Langmuir 2013, 29, 9369−9377

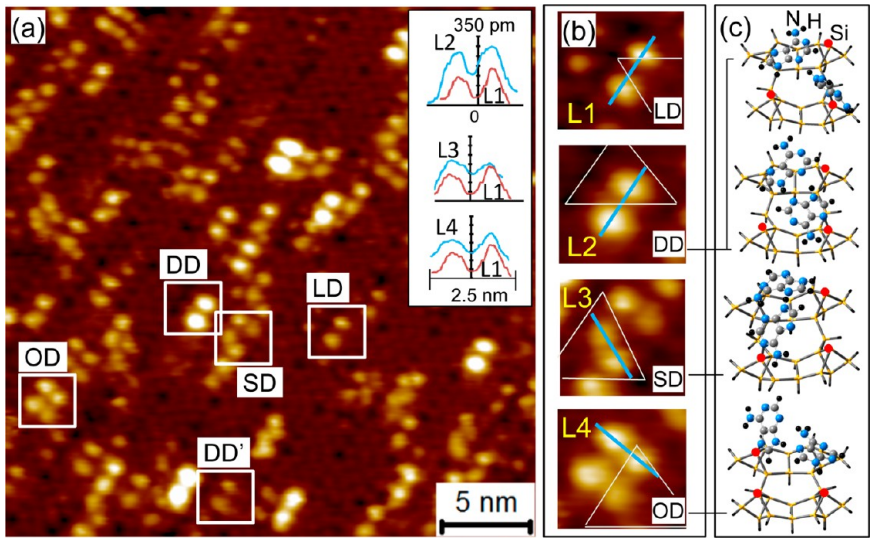

Figure 3. (a) Empty-state STM image (30 × 30 nm^2) of 15 s exposure of adenine on Si(111)7×7 recorded with a sample bias of +2 V and a tunneling current of 150 pA; (b) corresponding magnified STM images of selected adenine dimers including long dimer (LD), diagonal dimer (DD and DD′), side dimer (SD), and opposite dimer (OD) marked by open squares in (a); and (a, inset) the height profiles along linescans L2, L3, and L4 compared to that along L1; and (c) plausible equilibrium geometries for the DD, SD, and OD adenine dimers datively bonded to the $Si_{26}H_{24}$ cluster (with the adatoms marked by solid circles), as optimized by the DFT/B3LYP/6-31++G(d,p) method. The triangles in (b) outline the half-unit cells.

linear double or multiple dimers is expected to be a less stable unit.

Given the similar appearances for Ade on Si(111)7×7 in both empty-state and filled-state imaging modes, as illustrated in Figure 1, it is more straightforward to use empty-state images for the analysis of Ade adsorption.[37] Figure 3a shows a 30 × 30 nm^2 empty-state image for a 15 s exposure of Ade on Si(111)7×7. Evidently, a higher exposure of Ade gives rise to a much larger proportion of dimers than monomers when compared to, e.g., the 10 s exposure shown in Figure 1a. Closer examination reveals four types of dimers: long dimer (LD) with two Ade molecules adsorbed with a separation between 1.5 and 2 times the AA-to-CA distance (7.68 Å); diagonal dimer (DD) with two Ade molecules adsorbed at AA and CA diagonally across the dimer wall or at two CAs within a half unit cell; side dimer (SD) with both Ade adsorbed at adjacent adatoms on the same side of the dimer wall; and opposite dimer (OD) with both Ade adsorbed at either AA and AA or CA and CA directly across the dimer wall (Figure 3b). As shown in Figure 3a, the intensity of the bright protrusions for dimers could also vary quite notably because of the different tilt orientation of the Ade molecules inside the dimer, with the brighter protrusions corresponding to Ade molecules lying closer to the surface plane (more tilt, second top panel). The corresponding height profiles (Figure 3a, inset) show that the double peaks along L2 are stronger and broader than those along L1. The intensities for the LD, SD, and OD protrusions are usually found to be lower than the brightest DD protrusion (Figure 3b). Using the separation between the maxima of the height profiles along the appropriate linescans, we observe the separation follows the order LD (1.21 nm, along L1) > DD (1.15 nm, along L2) > SD (1.08 nm, along L3) > OD (1.05 nm, along L4), which is in good accord with the spatial separations between the respective surface atom pairs: diagonal AA-CA (1 nm) > same side AA-CA (0.7 nm) > opposite AA-AA or CA-CA (0.6 nm).

It should be noted that we have carefully examined the possibility of whether the observed dimer images could be artifacts caused by a double tip. This can be excluded because a double tip should cause every bright spot to appear as a set of double spots and clearly this is not the case here. Furthermore, the experiments have been carried out with different exposures and repeated several times with different STM tips. The presence of dimers (together with monomers appearing as single spots in the same image) and their chain formation along the equivalent dimer row directions have been consistently and reproducibly observed.

Figure 3c shows the plausible dimer ASCs of DD, SD, and OD on the $Si_{26}H_{24}$ cluster, with (N7, N7), (N1, N1), and (N1, N7) of the two Ade molecules forming the dative bonds with the appropriate adatom sites, respectively. We have not included calculations for LD ASCs because of the various possible configurations involving even larger Si clusters needed for the model surfaces. The "single" ASC calculations shown in Figure 1e suggest that dative bonding involving N3, N1, or N7 of a single Ade molecule to an adatom site are more likely. Using a combination of any two of these three datively bonded singles, we could obtain possible "flat" free dimer configurations as those shown in Figure 2 and these configurations are also summarized in Table 1. Interestingly, singles involving N1 and N7 dative bonding give rise to the more stable dimers (A, B1, B2), while dimers involving singles with N3 dative bonding are less stable. In order to obtain the possible dimer ASCs, the singles must undergo structural rearrangement from the "free" planar dimer configurations to appropriate substrate-modified nonplanar dimer configurations. These configurations accommodate dative bonding of the participating singles to the adatoms with the appropriate DD, SD, and OD geometries. Based on the dimerization energies of the free dimer configurations (Figure 2), we only consider the three most stable free dimer configurations (A, B1, and B2) as candidates for the substrate-modified dimer configurations, as shown in Table 1. Evidently, except for SD involving N1+N1 datively bonded singles, all other DD, SD, and OD involving N1 and N7 dative bonding favor the modified A geometry. The resulted

dx.doi.org/10.1021/la400775e | Langmuir 2013, 29, 9369−9377

Table 1. Plausible H-Bonding Arrangements of Free Dimers Consisting of Monomers Involving Selected N Atoms and of Substrate-Modified Dimer Configurations Involved in Different Types of Dative Bonding Arrangements: Diagonal Dimer (DD), Side Dimer (SD), and Opposite Dimer (OD)

N positions of the dative-bonded monomers	"free" dimer configurations	substrate-modified dimer configurations
N3+N3	C1 [N10−H···N1 and N1···H−N10]	[a]
	C2 [N10−H···N1 and N7···H−N10]	
	C3 [N10−H···N7 and N7···H−N10]	
N3+N1	B2 [N10−H···N3 and N7···H−N9]	[a]
	C3	
N3+N7	B2, C1, C2	[a]
N1+N1	A [N9−H···N3 and N3···H−N9]	Modified A for DD
	B2	Modified B2 for SD
	C3	Modified A, B2 for OD
N1+N7	A	Modified A for DD
	B1 [N10−H···N3 and N1···H−N9]	Modified A for SD
	B2	Modified A for OD
N7+N7	A, B1, C1	Modified A for DD
		Modified A, B1 for SD
		Modified A, B1 for OD

[a]Given the energies for the "free" dimer configurations, we only consider the top three most stable free dimer configurations (A, B1, and B2) for possible substrate-modified dimer configurations.

dimer ASCs could contain adsorbed Ade molecules with different tilts and twists as well as lateral positional rearrangement from one another, which could produce protrusions with different levels of brightness for the corresponding dimers (Figure 3a, DD vs DD′). Furthermore, within an individual optimized dimer ASC, the Ade molecules are also found to exhibit different amounts of tilt and twist from each other, which is consistent with the different peak shapes and maxima observed in the height profiles (Figure 3a, inset). For example, one of the peaks along L2 (for DD) is found to have a larger maximum and a smaller width than the other peak. A modified A dimer ASC with different tilts in the individual Ade molecules (Figure 3c, top two panels) can therefore be used to account for two different DDs with different bright protrusions (Figure 3a, DD vs DD′). Similarly, a modified A or B2 dimer ASC could correspond to the observed OD arrangement, while a modified A or B1 dimer ASC could account for the SD arrangement (Figure 3b, bottom two panels).

In addition to the dimers found for the higher exposure of Ade on Si(111)7×7 surface, we observe apparent self-organization of these dimers into linear double dimers, quartets, linear chains, and other higher-order superstructures. To understand the general nature of this self-organization, we illustrate in Figure 4 the H-bond mediated "links" between individual dimer units found in the self-organization of these superstructures on the 7×7 template for a 15 s exposure of Ade. In particular, two dimers can be linked in an end-to-end (ETE) arrangement (i.e., along the long axis of the dimer marked by

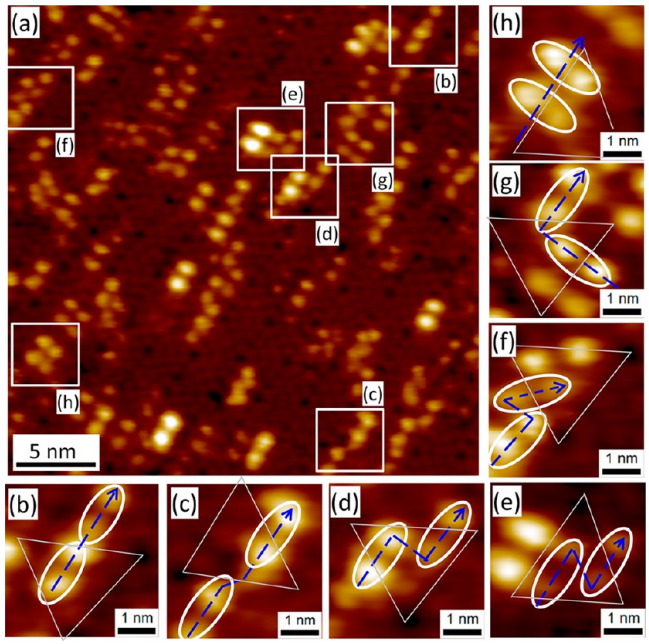

Figure 4. (a) Empty-state STM image (30 × 30 nm^2) of a 15 s exposure of adenine on Si(111)7×7 recorded with a sample bias of +2 V and a tunneling current of 150 pA, and magnified views of H-bond mediated links between different dimers in (b) direct end-to-end (ETE), (c) offset ETE, (d) 90° zigzag (ZZ90), (e) 60° zigzag (ZZ60), (f) wide-angle turn (WAT), (g) right-angle turn (RAT), and (h) side-by-side (SBS) arrangements, with the arrows marking the direction of growth and the triangles outlining the half unit-cells.

eclipse) near-linearly in two ways. Figure 4b shows a direct ETE configuration with one of the dimer protrusions being brighter than the other, which is likely due to different extents of the tilts in the two dimers. On the other hand, Figure 4c shows a slightly "offset" ETE configuration with equally bright protrusions for both dimers. The slight lateral offset is likely imposed by the H-bond alignment between two dimers with nearly equal amounts of tilts. Like the two ETE arrangements, the zigzag (ZZ) arrangements also involve one end of the dimer linked to another end of an adjacent dimer, except the link direction is no longer parallel to the long axis. For ZZ90 (Figure 4d), the angle between the link direction and the long axis is 90°, while this angle is 60° for ZZ60 (Figure 4e). For the ETE and ZZ arrangements, the growth direction of the second dimer (marked by the dashed line arrow) is parallel to the long axis of the first dimer (marked by the dashed line in Figure 4), without and with lateral offset. In addition, the growth direction could also undergo a wide (obtuse) angle turn (WAT, Figure 4f) or a right-angle turn (RAT, Figure 4g). Furthermore, the growth direction could also be perpendicular to the long axis of both dimers in a side-by-side (SBS) arrangement (Figure 4h). These seven link arrangements provide the basic mechanism for the observed chain-like growth. Of special interest is the remarkable alignment of the chains all along (−1 1 0) direction, indicating a strong surface template effect on the self-directed growth of these Ade dimers.

Figure 5 shows empty-state STM images for four Ade exposures on Si(111)7×7 during the early growth stage. Using the full 50 × 50 nm^2 images (of approximately 400 7×7 unit cells), we count the numbers of individual monomers or singles (S), dimers (D), selected double dimers such as ETE and SBS, and larger/longer dimer chains consisting of multiple dimers

dx.doi.org/10.1021/la400775e | Langmuir 2013, 29, 9369−9377

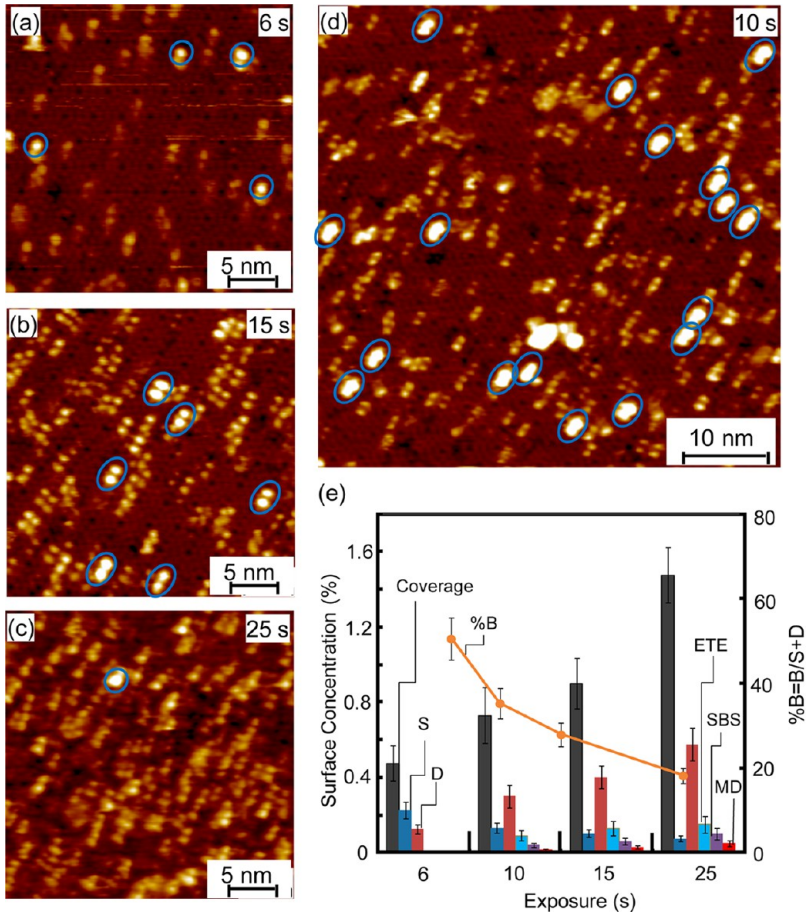

Figure 5. Empty-state STM images (50 × 50 nm^2) of (a) 6 s, (d) 10 s, (b) 15 s, and (c) 25 s exposures of adenine on Si (111)7×7 recorded with a sample bias of +2 V and a tunneling current of 150 pA, with (a), (b), and (c) shown with a magnified view (30 × 30 nm^2). (e) Corresponding relative surface concentrations for singles (S), doubles (D), end-to-end (ETE), side-by side (SBS), and multiple dimers (MD), along with the total coverage and the percentage of brighter protrusions in S+D (examples marked by ovals) and indicated as %B, all as a function of adenine exposure.

(MD), and their relative surface concentrations (i.e., the fractions of the available sites that are occupied by the respective Ade configurations) are presented in Figure 5e. Evidently, growth begins with just the S and D populations on the 7×7 surface for the 6 s exposure (Figure 5a), with the relative surface concentrations for S being higher than that for D (Figure 5e). As the exposure increases, the relative surface concentration for S decreases gradually while that for D increases (Figure 5e). For the 10 s exposure (Figure 5d), we also observe the emergence of double dimers and larger dimer chains, with their relative surface concentrations following the order: ETE > SBS > MD. The relative surface concentrations of ETE, SBS, and MD all appear to increase as the exposure is increased to 15 and 25 s (Figure 5e). The increase in the ETE occupancy appears to slow down while the increase in the SBS occupancy remains steady. This is consistent with the formation of double and multiple parallel chains becoming more prominent at a higher exposure. For exposures above 25 s (not shown), the 7×7 template is totally covered by Ade and accompanied with multilayer formation, which makes our statistical analysis difficult (due to the lack of the reference 7×7 template). In addition, with the exception of the very low exposure (i.e., 6 s), all other STM images for the higher exposures show remarkable alignment of the dimer chains along the [−1 1 0] direction. Even more interesting is that almost all the dimer chains are aligned along a particular direction (within the field of view of 50 × 50 nm^2), despite the threefold symmetry of the 7×7 half unit cell. While the exact mechanism of this self-alignment is not clear, we hypothesize that interchain interactions play an important role in orienting the neighboring dimers along a specific growth direction. Some of these interchain interactions are manifested in the H-bond mediated links shown in Figure 4. Moreover, most of the chains appear to be limited to a finite number of dimers for a particular exposure (e.g., Figure 5c), likely because of the surface template effect of the 7×7 surface (in contrast to the more homogeneous metal surface) and of the tilted dimer bonding geometry that is less compatible with horizontal growth parallel to the surface. In Figure 5e, we also show the total coverage of Ade on the 7×7 surface, which evidently increases almost linearly up to 25 s exposure. The number of occupied adatoms on the faulted half of the 7×7 unit cell is found to be almost the same as that of the unfaulted half for the four exposures (not shown), which is not surprising because of the dative bonding nature of the adsorption. Furthermore, the number of brighter protrusions (marked by ovals in Figure 5), with brightness similar to DD in Figure 3b, is found to decrease with increasing exposure (Figure 5e). This is consistent with the geometry of dimers becoming less tilted (i.e., more vertical) at a higher exposure due to steric interactions.

dx.doi.org/10.1021/la400775e | *Langmuir* 2013, 29, 9369−9377

4. CONCLUSION

The early growth stage of Ade on Si (111)7×7 has been studied by STM. Both the empty-state and filled-state images show bright protrusions without any evidence of dissociation, which indicates molecular adsorption of Ade through dative bonding, in good accord with our recent XPS results. Variation in the brightness of the protrusions is observed and can be attributed to the extent of the molecular tilt with respect to the surface normal. Of particular interest is the unique site-specific information about the early adsorption of Ade on the 7×7 surface provided by the present work. In particular, above 6 s exposure, the observed protrusions predominantly appear as dimers, which indicates that hydrogen bonding interactions between Ade molecules play a prominent role in the initial adsorption and subsequent growth process. From the DFT/B3LYP/631++G(d,p) calculations for free H-bond mediated Ade dimers, we expect dimers involving N9—H···N3 and N3···H—N9 H-bonds (A in Figure 2), and N10—H···N3 and either N1···H—N9 (B1) or N7···H—N9 (B2) to provide the most stable dimer configurations on the surface. Our STM images obtained at a higher exposure further reveal the different adsorption arrangements of the Ade dimers with the Si adatoms on the 7×7 surface, including long dimers, diagonal dimers, side dimers, and opposite dimers. Using a model surface based on the $Si_{26}H_{24}$ cluster, we also demonstrate the plausible adsorption substrate configurations of these adsorbed Ade dimers on adatoms across a Si dimer wall. At 15 s Ade exposure, the dimers are found, for the first time, to undergo self-organization into aligned superstructures, including straight, offset, and zigzag chains, square quartets, double quartets, and other multiple dimer structures. We identify the common types of links in forming these dimer superstructures, including end-to-end (both direct and offset), 90° and 60° zigzags, wide-angle and right-angle turns, and side-by-side arrangements. The end-to-end growth is found to be the most prominent especially in the initial growth stage, which leads to the formation of dimer chains. At 25 s exposure, dimer chains appear to grow side by side, remarkably all aligned in the same direction within a field of view of 50 × 50 nm^2. While the exact mechanism of this self-aligned growth is unclear, we believe that interdimer hydrogen bonding interactions may play an important role. We are currently conducting more detailed computational studies involving model surfaces with several complete 7×7 unit cells to decipher the nature of this self-organization. The observed self-aligned growth of Ade on Si(111)7×7 promises exciting applications in molecular electronics and photonics (such as molecular grating), lithography, and biomolecular sensing.

■ ASSOCIATED CONTENT

Ⓢ Supporting Information

XPS data for Adenine on Si(111)7×7. This material is available free of charge via the Internet at http://pubs.acs.org.

■ AUTHOR INFORMATION

Corresponding Author

*E-mail: tong@uwaterloo.ca.

Notes

The authors declare no competing financial interest.

■ ACKNOWLEDGMENTS

This work was supported by the Natural Sciences and Engineering Research Council of Canada.

■ REFERENCES

(1) Leftwich, T.; Teplyakov, A. Chemical manipulation of multifunctional hydrocarbons on silicon surfaces. *Surf. Sci. Rep.* **2007**, *63*, 1−71.

(2) Bent, S. F. Organic functionalization of group IV semiconductor surfaces: principles, examples, applications, and prospects. *Surf. Sci.* **2002**, *500*, 879−903.

(3) Ebrahimi, M.; Chong, J. M.; Leung, K. T. Selective Adsorption and Thermal Evolution of Bifunctional Carboxylic Acids: Competition of O-H Dissociation and Other Reaction Products in Acrylic Acid and Propanoic Acid on Si (100)2×1. *J. Phys. Chem. C* **2010**, *114*, 2947−2957.

(4) Radi, A.; Ebrahimi, M.; Leung, K. T. Relative reactivities of amino and ethenyl groups in allylamine on Si(100)2×1: Temperature-dependent X-ray photoemission and thermal desorption studies of a common linker molecule. *Elsevier B.V., Surf. Sci.* **2010**, *604*, 1073−1081.

(5) Zhang, L.; Chatterjee, A.; Ebrahimi, M.; Leung, K. T. Hydrogen-bond mediated transitional adlayer of glycine on Si(111)7×7 at room temperature. *J. Chem. Phys.* **2009**, *130*, 121103.

(6) Li, Q.; Leung, K. T. Thermally induced chemistry and electron-mediated processes of pyridine on (2×1) and modified Si(1 0 0) surfaces: evidence of electron-induced condensation oligomerization. *Surf. Sci.* **2003**, *541*, 113−127.

(7) Zhou, X. J.; Leung, K. T. Competition between associative and dissociative adsorption of 1,2-dihalogenated benzenes on Si(100)2×1: Formation of dihalocyclohexadiene, halophenyl and phenylene adstructures. *Surf. Sci.* **2006**, *600*, 3285−3296.

(8) Northrup, J. E. Origin of Surface States on Si(111)7×7. *Phys. Rev. Lett.* **1986**, *57*, 154−157.

(9) Tao, F.; Xu, G. Q. Attachment chemistry of organic molecules on Si(111)-7×7. *Acc. Chem. Res.* **2004**, *37*, 882−93.

(10) Huang, J. Y.; Huang, H. G.; Lin, k. Y.; Liu, Q. P.; Sun, Y. M.; Xu, G. Q. The structures of physisorbed and chemisorbed formic acid on Si(111)-7×7. *Surf. Sci.* **2004**, *549*, 255−264.

(11) Tanaka, K.-I.; Xie, Z.-X. Adsorption kinetics and patterning of a Si(111)-7×7 surface by dissociation of methanol. *J. Chem. Phys.* **2005**, *122*, 54706.

(12) Shimomura, M.; Sanada, N.; Fukuda, Y.; Moller, P. Highly site-selective adsorption of trimethylphosphine on a Si(111)-(7×7) surface studied by a scanning tunneling microscope (STM). *Surf. Sci.* **1995**, *341*, L1061−L1064.

(13) Yuan, Z. L.; Chen, X. F.; Wang, Z. H.; Yong, K. S.; Cao, Y.; Xu, G. Q. Dissociative adsorption of pyrrole on Si(111)-(7×7). *J. Chem. Phys.* **2003**, *119*, 10389.

(14) Cao, Y.; Yong, K. S.; Wang, Z. H.; Deng, J. F.; Lai, Y. H.; Xu, G. Q. Cycloaddition chemistry of thiophene on the silicon (111)-7×7 surface. *J. Chem. Phys.* **2001**, *115*, 3287.

(15) Yong, K. S.; Zhang, Y. P.; Yang, S.-W.; Wu, P.; Xu, G. Q. Studies of chemisorbed tetracene on si(111)-7×7. *J. Phys. Chem. A* **2007**, *111*, 12266−74.

(16) Yong, K.; Zhang, Y.; Yang, S.; Xu, G. Naphthalene adsorption on Si(111)-7×7. *Surf. Sci.* **2008**, *602*, 1921−1927.

(17) Chatterjee, A.; Zhang, L.; Leung, K. T. Direct Imaging of Hydrogen Bond Formation in Dissociative Adsorption of Glycine on Si (111) 7×7 by Scanning Tunneling Microscopy. *J. Phys. Chem. C* **2012**, *116*, 10968.

(18) Cysewski, P. An ab initio study on nucleic acid bases aromaticities. *J. Mol. Struct.* **2005**, *714*, 29−34.

(19) Tabata, H.; Kawai, T.; K., M. Scanning Tunneling Microscopy observation and theoretical calculation of the adsoption of adenine on Si(100)2×1 surfaces. *Surf. Sci.* **1995**, *342*, 215−223.

(20) kawai, T.; Tabata, H.; K., M. Scanning tunneling microscopy and molecular orbital calculation of thymine and adenine molecules

adsorbed on the Si(100)2×1 surface. *Surf. Sci.* **1996**, *357*−*358*, 195−201.
(21) Furukawa, M.; Tanaka, H.; Kawai, T. The role of dimer formation in the self-assemblies of DNA base molecules on Cu(111) surfaces: A scanning tunneling microscope study. *J. Chem. Phys.* **2001**, *115*, 3419.
(22) Chen, Q.; Frankel, D. J.; Richardson, N. V. Self-Assembly of Adenine on Cu(110) Surfaces. *Langmuir* **2002**, *18*, 3219−3225.
(23) Chatterjee, A.; Zhang, L.; Leung, K. T. Bidentate Surface Structures of Glycylglycine on Si(111)7×7 by High-Resolution Scanning Tunneling Microscopy: Site-specific Adsorption via N−H and O−H or Double N−H Dissociation. *Langmuir* **2012**, *28*, 12502.
(24) http://webbook.nist.gov/chemistry. *NIST Chemistry WebBook*.
(25) Frisch, M. J.; Trucks, G. W.; Schlegel, H. B.; Scuseria, G. E.; Robb, M. A.; Cheeseman, J. R.; Scalmani, G.; Barone, V.; Mennucci, B.; Petersson, G. A.; Nakatsuji, H.; Caricato, M.; Li, X.; Hratchian, H. P.; Izmaylov, A. F.; Peralta, J. A.; Peralta, J. E.; Ogliaro, F.; Bearpark, M.; Heyd, J. J.; Brothers, E.; Kudin, K. N.; Staroverov, V. N.; Kobayashi, R.; Normand, J.; Raghavachari, K.; Rendell, A.; Burant, J. C.; Iyengar, S. S.; Tomasi, J.; Cossi, M. *Gaussian 09*; Gaussian, Inc., 2009, .
(26) Becke, A. D. Density-functional thermochemistry. III. The role of exact exchange. *J. Chem. Phys.* **1993**, *98*, 5648−5652.
(27) Lee, C.; Yang, W.; R. G., P. Developement of the Colle-Salvetti correlation-energy formula into a functional of the electron density. *Phys. Rev. B* **1988**, *37*, 785−789.
(28) Tao, F.; Qiao, M.; Li, Z.; Yang, L.; Dai, Y.; Huang, H.; Xu, G. Adsorption of phenylacetylene on Si(100)-2×1: Reaction mechanism and formation of a styrene-like π-conjugation system. *Phys. Rev. B* **2003**, *67*, 1−7.
(29) Wolkow, R. A. Controlled Molecular Adsorption on Silicon: Laying foundation for Molecular devices. *Annu. Rev. Phys. Chem.* **1999**, *50*, 413−441.
(30) Hobza, P.; Sponer, J. Structure, energetics, and dynamics of the nucleic Acid base pairs: nonempirical ab initio calculations. *Chem. Rev.* **1999**, *99*, 3247−76.
(31) Asturiol, D.; Duran, M.; Salvador, P. Intramolecular Basis Set Superposition Error Effects on the Planarity of DNA and RNA Nucleobases. *J. Chem. Theory Comput.* **2009**, *5*, 2574−2581.
(32) Takahashi, S.; Takahashi, M.; Tanishiro, Y.; Takayanagi, K. Structural analysis of Si(111)7×7 by UHV-transmission electron diffraction and microscopy. *J. Vac. Sci. Technol., A* **1985**, *3*, 1502−1506.
(33) Lee, H. S.; Choi, C. H. Cluster study of surface radicals of Si(111)-7×7 reconstructed surface. *Theor. Chem. Acc.* **2007**, *120*, 79−83.
(34) Cordell, R.; Boggs, E. Structure and degree of aromatic character in Furan, Pyrrole and Thiophene. *THEOCHEM* **1981**, *85*, 163−178.
(35) Dunphy, J.; Rose, M.; Behler, S.; Ogletree, D.; Salmeron, M.; Sautet, P. Acetylene structure and dynamics on Pd(111). *Phys. Rev. B* **1998**, *57*, R12705−R12708.
(36) Preuss, M.; Bechstedt, F. Self-assembly of adenine-dimer chains on Cu(110): Driving forces from first-principles calculations. *Surf. Sci.* **2008**, *602*, 1643−1649.
(37) Wiesendanger, R. *Scanning Probe Microscopy and Spectroscopy: methods and application*; Cambridge University Press, 1994; pp 144−45.